Final Technical Report for DE-FG02-05ER15753

Asymmetric Semiconductor Nanorod/Oxide Nanoparticle Hybrid Materials: Model Nanomaterials for Light-Activated Formation of Fuels from Sunlight

PI: Dr. Neal Armstrong

09/01/2005 to 08/31/2016

University of Arizona

Final Technical Report -- Award DE-FG02-05ER15753

The above referenced award DE-FG02-05ER15753, was renewed on August 1, 2011. A close-out grant and a no-cost extension were granted to bring the end-date of this effort to August 31, 2016. This report details progress through August 31, 2016.

Executive Summary on Project Accomplishments: We focused our efforts for this project on the synthesis and characterization of semiconductor nanomaterials composed of semiconductor nanorods (NRs - e.g., CdSe, CdSe@CdS, CdS) with metal (Au, Pt, Co) or metal oxide (Co_xO_y) nanoparticle (NP) "tips." These systems are attractive model systems where control of spatial, energetic and compositional features of both NRs and NP tips potentially enhances the efficiency of photogeneration and directional transport of charges, and photoelectrochemical conversion of sunlight to fuels. Synthetic methods to control material dimensions (20-200 nm in length), topology (one vs. two NP tips) and NR/NP tip compositions have been developed in the current project period (**Pyun**). We also achieved, for the first time in heterostructured nanorod materials, estimates of both valence band energies (E_{VB}) and conduction band energies (E_{CB}), using unique combinations of *in vacuuo* ultraviolet photoelectron spectroscopy (UPS, **Armstrong**), and waveguide spectroelectrochemistry (**Saavedra**), respectively. The spectroelectrochemical measurements in particular provide a unique path to estimation of E_{CB} , and the distribution in E_{CB} brought about by modification of NR composition. The combination of both approaches promises to be universally applicable to the characterization of energetics in nanomaterials of interest both for photovoltaic and sunlight-to-fuel photoelectrochemical assemblies.

Project Background. Research products (18 publications) resulting from DOE support for this program (2007-15) are described at the end of this report.

Over the past decade, we have systematically explored new ways of building and characterizing nanometer-scale material constructs that provide for efficient photo-induced charge separation, are asymmetrically composed in a way as to ensure

for vectoral charge transfer, and more recently, decorated with metal and metal oxide catalytic sites, to enhance rates of photoelectrochemical "fuel-forming" processes over competing recombination events.

Our initial material involved electrochemically deposited **PEDOT** nanocomposite films decorated with CdSe NPs, capped with electron-rich thiophene ligands. (Fig. 1a). While these initial studies demonstrated that absorbed-photon to current efficiencies (APCE) were high, and correlated with band edge energies of the NP (related to NP diameter), they also demonstrated the need sophisticated light for more absorbing, asymmetric nanomaterials. where absorption could be coupled with catalysts designed to accelerate OER (e.g. cobalt oxides), or HER (e.g. metal nanoparticles), and for a much more detailed approach to determination of band edge energies, which ultimately control the rates of HER and OER in

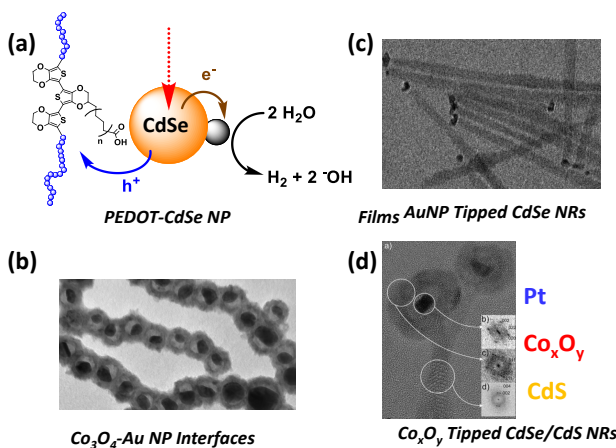


Fig. 1: Progression of our development of new photoactive NP or NR materials, tethered to conducting polymer films (a), formation of linked Co_xO_y NPs using Au seeds (b), and NRs tipped with metal or metal oxide nanoparticles (c,d) to introduce the kind of compositional asymmetry required to induce charge separation and efficient photocatalytic formation of fuels from sunlight.

any water splitting and/or fuel-forming system. This further led us to explore cobalt oxide-based

nanomaterials which we demonstrated are capable of electrocatalytic OER, particularly when coupled with noble metal inclusions, such as Au or Pt NPs (Fig. 1b)

We next focused on the development of new semiconductor nanorods (both CdS and CdSe) decorated with either metal or metal oxide tips, both symmetrically and asymmetrically, to create a family of nanocomposite materials capable of directing charge transport by spatial, compositional and energetic control within the nanomaterial (**Fig. 1c,d**). There have been few systematic studies of how NR composition and dimensions, the nature of capping ligands, and modification with catalytic sites affects band edge energies and electronic coupling to an underlying contact (that manifests as differences in rates of heterogeneous charge injection/extraction). As shown below we coupled these synthetic advances with new and quite unique spectroelectrochemical approaches to the characterization of both E_{CB} and rates of heterogeneous electron transfer as a function of NR composition, and UPS characterization of E_{VB} and preliminary studies of defect density of states (DOS) above E_{VB}.

1) Formation of new semiconductor nanorods with metallic and oxide catalytic tips:

We created a series of unique semiconductor NR materials (either CdSe@CdS, CdS, or CdSe) that have been tipped at either one end or both ends with catalytic sites, either metals (Pt, Au) or oxides such as Co_xO_y. The distinguishing feature of the synthetic aspects of this work was development of reproducible and scalable methods to enable the preparation of materials in sub-gram quantities (100-900 mg). The vast majority of reports in synthetic nanochemistry fail to report basic aspects of the synthesis, such as purification and yield. Furthermore, the access to these semiconductor nanomaterials in these quantities enabled the total synthesis of complex nanocomposite materials for the first

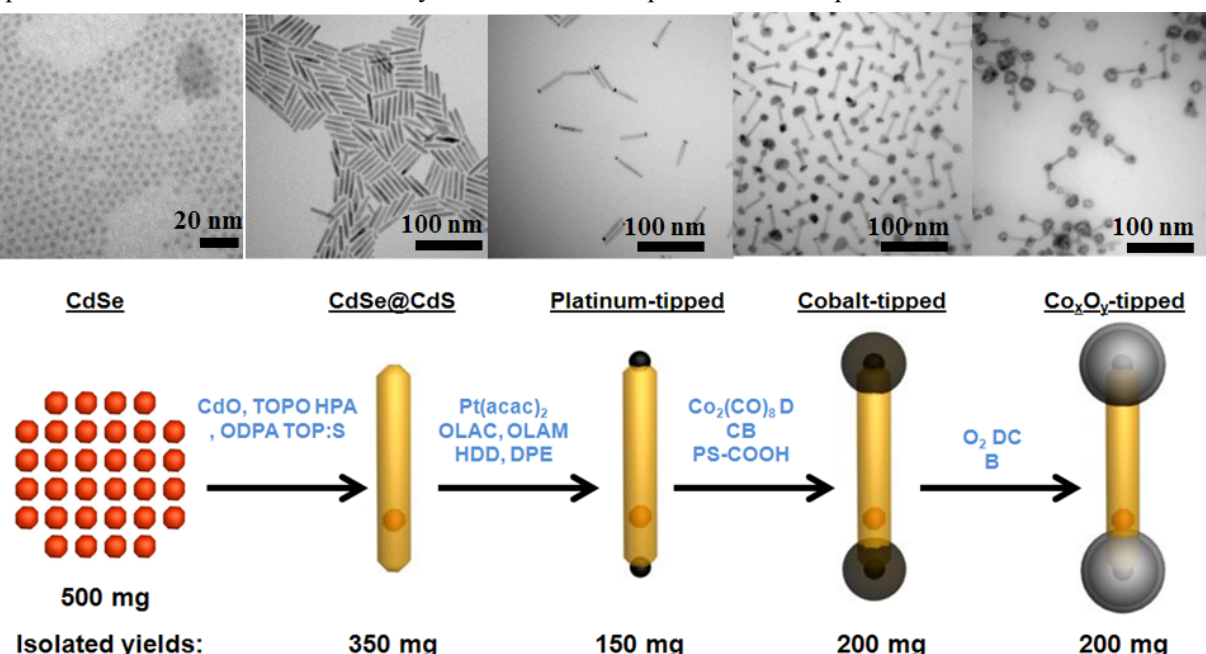


Fig 2: Five-step synthesis of CoxOy-tipped nanorods with dumbbell morphology. CdSe quantum dot seeds (D = 2.3-2.7 nm) were used to form heterostructured CdSe@CdS nanorods of varying length (40-174 nm). Pt NP deposition onto CdSe@CdS nanorod termini was then conducted for the series of CdSe@CdS nanorods to enable cobalt deposition. Selective oxidation of cobalt-tipped nanorods afforded the final product. Abbreviations: (TOPO) trioctylphosphine oxide, (TOP) trioctylphosphine, (HPA) n-hexylphosphonic acid, (ODPA) n-octadecylphosphonic acid, (OLAC) oleic acid, (OLAM) oleylamine, (HDD) 1,2-hexadecanediol, (DPE) diphenylether, (PS-COOH) carboxylic acid-terminated polystyrene, (DCB) 1,2-dichlorobenzene.

time. Heterostructured NRs based on CdSe@CdS have served as model systems to develop these synthetic methods, with an emphasis on installing one or two NP tips per NR. In our initial work, we determined the key feature is the ability to control the deposition of either Au or Pt NP tips onto semiconductor CdSe@CdS NRs. The presence of the noble metal seeds enabled quantitative deposition of metallic Co NP tips, which were readily oxidized to form Co_xO_y tips that were still intact on the nanorod (**Fig. 2**). The approach proved to be high modular and readily applied to other NR materials (CdS, CdSe) to enable spatial and energetic control in the photoactive nanocomposite. We also prepared heterostructured CdSe nanorods that incorporate Au, Co and Co_xO_y tips. CdSe NRs are useful model constructs because they have high bandgap energies and afford ease of synthesis and tuning of the NR size, shape and functionalization in numerous ways, which leads to insights about their energetics that should be generalizable across a number of material platforms. Figure 1c shows a recent TEM characterization of individual NRs, Au-tipped NRs and Au-NR fused assemblies which show intriguing linkages between NRs which, if controlled, might lead to vectoral charge transport – a prerequisite for photoelectrocatalytic assemblies.

2) Characterization of valence band energies in NCs and NRs using photoemission spectroscopies; effect of metallic tips on E_{VB} :

We developed a unique approach to the characterization of E_{VB} in ultra-thin films of NCs and NRs using UV-photoemission spectroscopies (He I and He II UPS), providing greater confidence in the energies of these band edges, especially relative to previous PES studies of related systems. These improvements also gave us confidence that we can use high sensitivity, high dynamic range forms of these UPS experiments to characterize mid-gap defect DOS in new NR materials. For NR materials based on semiconductors such as CdSe and CdS, we observed large shifts in local vacuum level (as a result of the strongly dipolar nature of these II-VI nanomaterials) and large photoemission backgrounds resulting from secondary electron scattering (**Fig. 3**). Correcting for these effects is especially critical for monitoring the differences in E_{VB}/E_{CB} that result from changes in NR composition, length and tipping chemistries.

Fig. 3 summarizes the photoemission spectra for several different NR constructs, examined for the first time by this approach. Each of these materials was deposited on freshly cleaved highly ordered pyrolytic graphite (HOPG), which produces a much lower photoemission background in regions which are critical for determination of valence band energies, versus previous studies where the NP or NR was tethered to metal surfaces such as Au, where background photoemission made absolute determination of E_{VB} problematic. In Fig. 3, the low kinetic energy edges (LKE) show significant shifts as NR size and composition are varied. To determine high KE (HKE) photoemission edge energies, we now systematically remove He-satellite photoemission peaks and secondary electron scattering backgrounds – the resultant $E_{VB} = 21.1 \text{ eV} - (\text{HKE} - \text{LKE})$ is much more clearly defined than in previous photoemission studies. E_{CB} is subsequently estimated using the optical band gap of the NR. Band edge energies derived from photoemission experiments are summarized in Fig. 3B. There are significant decreases in E_{VB} relative to vacuum (and E_{CB}) for Au-tipping of CdSe NRs, which is predicted to increase the driving force for HER and lower the driving force for OER, and will factor into the design of new semiconductor nanomaterials.

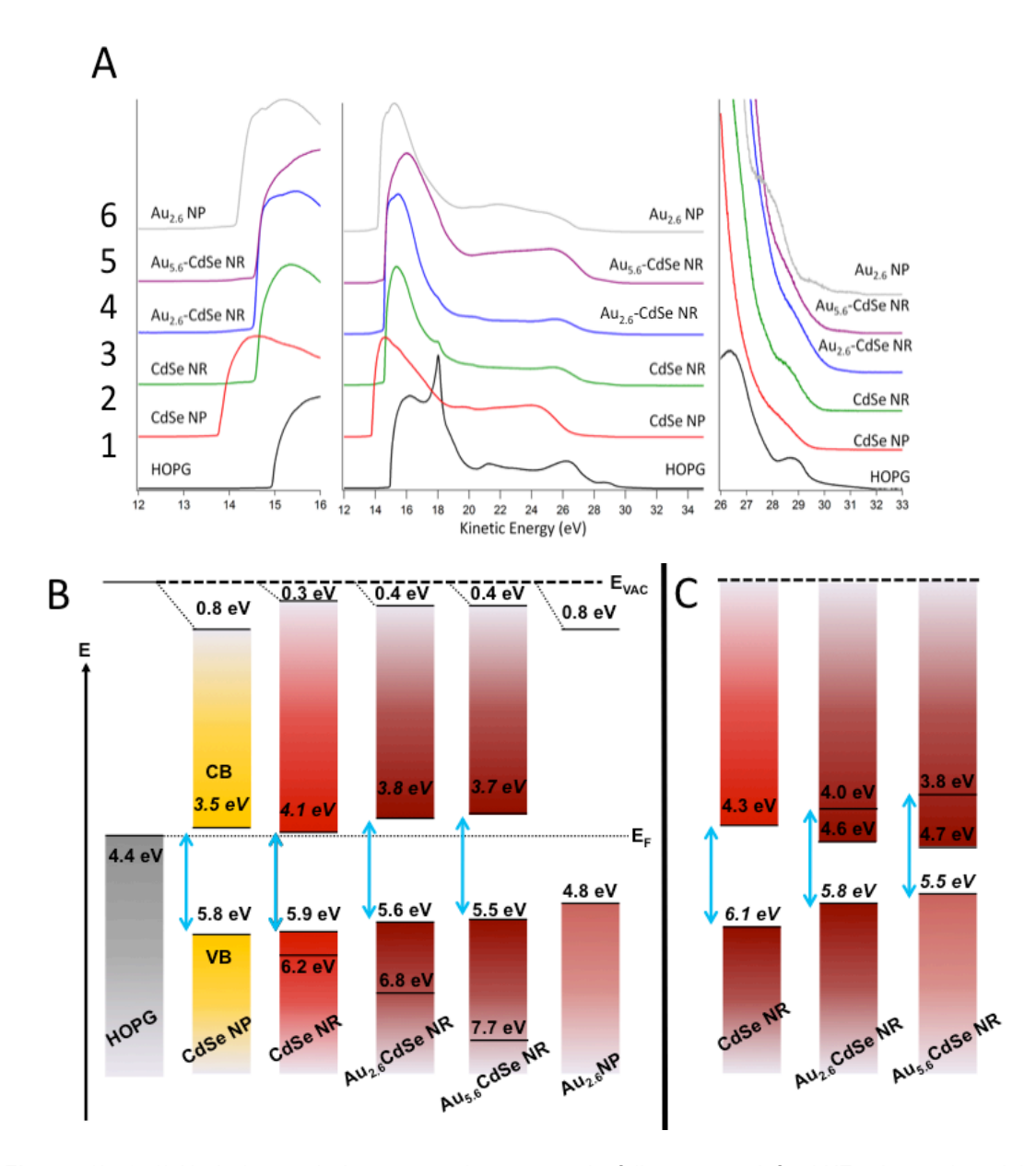


Fig. 3: (A: 1-6)) He I photoemission spectra (center panel - full spectrum; left - LKE edge region; right - HKE edge region) for the HOPG substrate, the CdSe NP seed, CdSe NRs grown from the seed, NRs tipped with 2.6 and 5.6 nm Au NPs, and isolated Au NPs as a reference material. Significant shifts in LKE are observed among these materials, arising from their strongly dipolar character. New approaches to treatment of the HKE spectral region, include: i) the use of HOPG substrates that minimize spectral background in these critical regions; and ii) the removal of both He I satellite contributions and secondary electron scattering background, leading to greater confidence in determination of E_{VB} , summarized in (B). Once E_{VB} has been estimated, E_{CB} is derived using the optical gap (blue arrow) of each NP or NR. (C) Summary of the band edges estimated from spectroelectrochemical data, corrected to the vacuum scale (see below). Once E_{CB} has been estimated from the onset for electron injection into the NR, E_{VB} is derived from the optical band gap.

3) Waveguide-based spectroelectrochemical characterization of conduction band energies and rates of heterogeneous ET in CdSe NRs with Au NP Tips

In a previous funding period, we demonstrated the use of waveguide-based spectroelectrochemistry to monitor electron injection into the conduction band of NCs tethered to surfaces of semitransparent oxides (ITO) in contact with electrolyte. We extended these studies to bare and Au-tipped CdSe NRs. Example data for a CdSe NR monolayer film (length (L) = 40.1 nm, diameter (D) = 9.6 nm, grown from CdSe seed) adsorbed on an ITO-coated waveguide electrode derivatized with 1,8-octanediphosphonic acid (OdiPA) are shown in **Fig. 4**. As the applied potential is stepped negative (toward the vacuum level; Fig. 4A), electron injection into the NR film causes bleaching of the lowest energy excitonic features (Fig. 4B). Plotting dA vs V at select wavelengths (Fig. 4C) provides estimates of the onset potentials for injection into the $I\Sigma_e$ and $I\Pi_e$ levels of the CdSe NR conduction band. To convert onset potentials to the vacuum scale, the potential of the normal hydrogen electrode (NHE) vs. vacuum was taken to be -4.48 eV. The mid-point potential of the ferrocene/ferricenium (Fc/Fc⁺) redox couple used to calibrate the Ag/AgNO₃ (0.01M) reference electrode was 0.07 V. The potential of Fc/Fc⁺ was taken to be 0.64 V vs NHE and E_{CB} values were therefore estimated from $E_{CB} = -(E_{red} + 5.05)$ eV, where E_{red} is the measured onset potential. This treatment yielded the E_{CB} values shown in Fig. 3C.

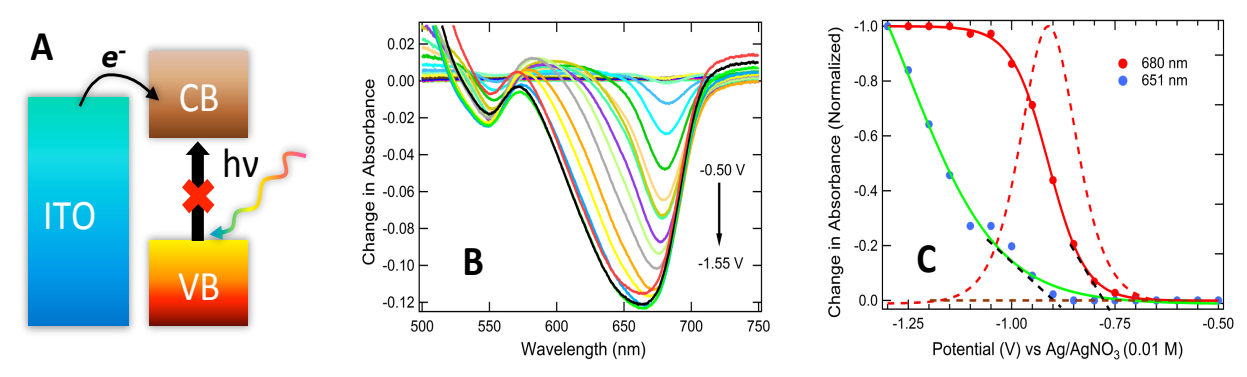


Fig. 4 – (A) Schematic of bleaching that accompanies electron injection into the conduction band of a NR electrochemically coupled to ITO as the electrode potential is stepped closer to vacuum. (B) Potential-controlled ATR difference spectra showing progressive bleaching as a function of potential (vs Ag/AgNO₃) applied to a CdSe NR film on a OdiPA-modified, ITO-coated waveguide; (C) Difference absorbance (normalized) vs V at peak wavelengths for the two major bleaching bands in B; sigmoidal fits to the data (solid lines) were used to estimate the onset potentials (black dashed lines) for injection into the $1\Sigma_e$ and $1\Pi_e$ levels of the CdSe conduction band.

The dA vs V plot for an adsorbed film composed of CdSe NRs functionalized with 2.6 nm Au tips is shown in Fig. 5. It contains two distinct regions, indicative of two distinct bleaching processes that are assigned to electron injection into metal-semiconductor interface (MSI) states (i.e., sub-gap states) and the $I\Sigma_e$ level of the CdSe NR conduction band. The $I\Sigma_e$ level is shifted closer to vacuum, relative to bare NRs, because multiple electrons are injected into the ensemble of levels in a single NR: at less negative potentials, charges are injected into both single electron tunneling (SET) levels (i.e., the Coulomb staircase) in the Au NP tips, as well as the MSI states; at more negative potentials, charges are injected into the $I\Sigma_e$ level of the NR conduction band. Filling the SET levels and MSI states charges the NR, shifting the apparent onset E_{CB} to more negative potentials (see band diagram in Fig. 3C). These data are the first reported quantitative measurements of absolute energy levels for any type of semiconductor NR.

The heterogeneous ET kinetics of these NR films were investigated using potential-modulated ATR (PM-ATR) spectroelectrochemistry. In PM-ATR, the potential applied to the ITO electrode is modulated while the real and imaginary components of the ATR signal are monitored. The measurement is performed as a function of modulation frequency, from which the heterogeneous charge transfer rate

constant $(k_{s,opt})$ for electron injection/extraction to/from the spectroelectrochemically active film is obtained. The $k_{s,opt}$ values for CdSe and Au(2.6 nm)-tipped CdSe NR films were $2.5(\pm 0.8) \times 10^3$ s⁻¹ and $1.4(\pm 0.1) \times 10^4$ s⁻¹, respectively. The increase in $k_{s,opt}$ upon Au tipping is indicative of enhanced electronic coupling of the NR film to the ITO electrode, and is consistent with our interpretation of the spectrelectrochemical data presented in Figs. 4-5.

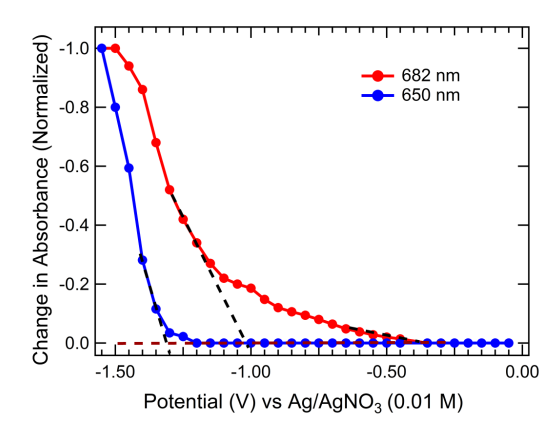


Fig. 5 – Potential-dependent bleaching of a monolayer of Autipped CdSe NRs adsorbed on a OdiPA-modified, ITO-coated waveguide. Plotted here is the difference absorbance (normalized) vs V at the peak wavelength of the two major bands in the difference spectra (not shown). The black dashed lines are extrapolations from the two bleaching transitions apparent in the 682 nm curve, from which onsets of ca. -0.4 V for injection into MSI states and ca. -1.0 V for injection into the $1\Sigma_e$ level of the CdSe conduction band were determined.

In rationalizing the differences between the spectroelectrochemical characterization data and the photoemission data, it is important to note that in UPS, photoemission is detected from the uppermost 1-3 nm of a NR film. If the NR diameter is ca. 9 nm, NR bulk energetic properties will certainly not be emphasized in the photoemission spectra, nor will effects due to NR-substrate electronic coupling. In the waveguide ATR geometry, the entire film thickness is optically sampled; when combined with electrochemistry, the fraction of the NR film that is electrochemically coupled to the waveguide electrode is probed. Furthermore, the spectroelectrochemical measurements are not corrected for local vacuum level shifts; it is assumed that the working and reference electrodes are at the same local vacuum level. Given these differences, the E_{VB}/E_{CB} levels obtained by UPS and spectroelectrochemistry are expected to differ, however, the trends in the E_{VB}/E_{CB} shifts as a function of NR structure and composition are expected to be similar, as we have demonstrated for bare and Au-tipped CdSe NRs (compare Figs. 3B and 3C).

4) Spectroelectrochemical characterization of Co_xO_y NP tipped Semiconductor NRs

More recently, we performed spectroelectrochemical studies of "matchstick" Co_xO_y -tipped CdSe NRs (**Fig. 6**). Potential-dependent bleaching spectra of a submonolayer of these NRs (L =40 nm, D = 5 nm, D of tip = 6 nm) are shown in Fig. 6B. Bleaching spectra were also acquired for the precursor bare CdSe rods (not shown). The dA vs V plots (Fig. 6C-D) show that the addition of the Co_xO_y shell on the NP tip significantly affects the bleaching behavior. The curve for the bare CdSe NR sample shows the expected steep onset that corresponds to conduction band edge. The curve for the Co_xO_y -tipped NRs has a very similar onset but the potential range over which electron injection occurs is considerably broader, with the distribution of energy levels shifted towards vacuum. This shift is interpreted as: The Co_xO_y shell blocks electron injection directly into the SET levels and MSI states associated with the Au NP. When the potential is sufficiently negative, injection occurs into the CdSe conduction band which also fills the SET levels and MSI states. At more negative potentials, injection into the Co_xO_y conduction band occurs. The partially overlapping distribution of energy levels in the CdSe and Co_xO_y conduction bands gives rise to the broad curve in Fig. 6D. These data demonstrate electrochemical coupling between ITO and Co_xO_y -tipped NRs and, along with the data for Au-tipped CdSe NRs presented above, represents the first determination of conduction band energies for any heterostructured NR system.

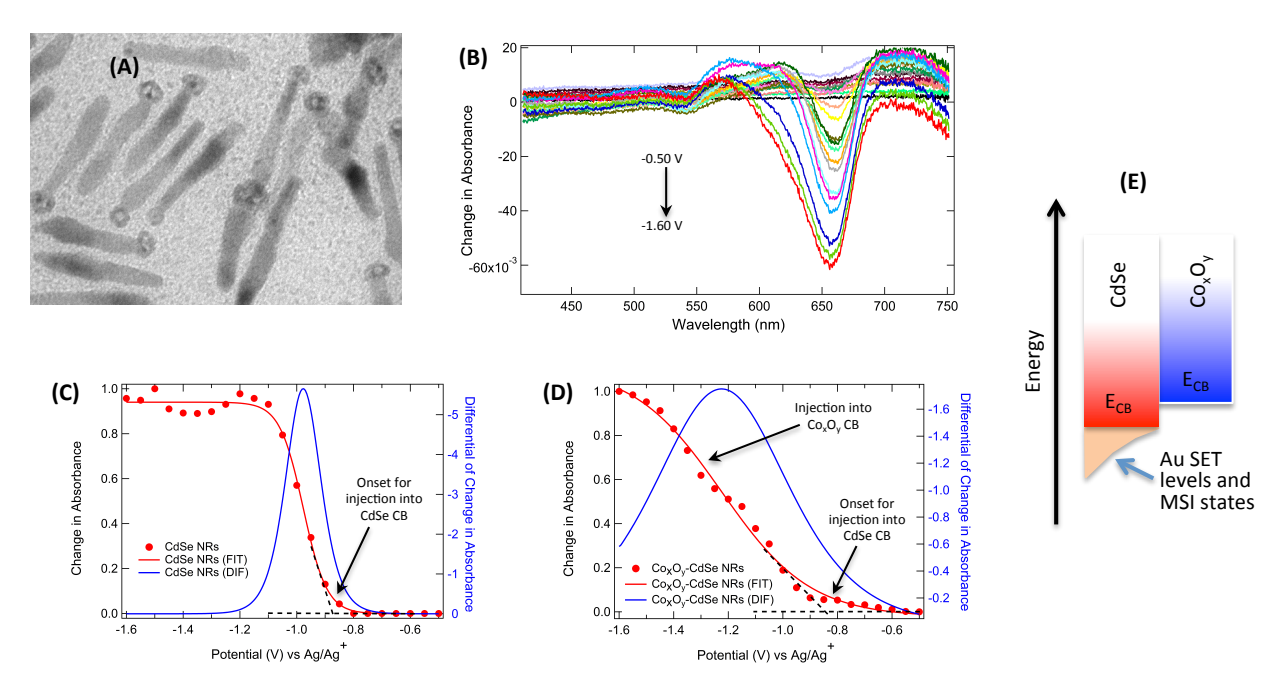


Fig. 6 – (A) TEM image of "matchstick" Co_xO_y NP-tipped NRs. (B) Potential-controlled ATR difference spectra showing progressive bleaching as a function of potential (vs Ag/AgNO₃) applied to a film of Co_xO_y NP-tipped NRs on a OdiPA-modified, ITO-coated waveguide. In (D), the difference absorbance (normalized) vs V at the peak wavelength of the longest wavelength bleaching band for the Co_xO_y -tipped NR film is plotted; the corresponding data for a film of the precursor (bare) CdSe NRs is shown in (C). The solid red lines are sigmoidal fits to the data and the solid blue lines are first derivative plots to show the width of the transitions. The dashed black lines show the onset potential for injection is the same for both films. (E) Energy level diagram for the Co_xO_y NP-tipped NR film. Both the CdSe NR and the Co_xO_y shell are in electrochemical contact with the ITO. The Co_xO_y shell blocks direct injection into the SET levels and MSI states associated with the Au NP, which occurs in the absence of the Co_xO_y shell (see Fig. 5). When the potential is sufficiently negative, injection into the CdSe CB occurs, which also fills the SET levels and MSI states. At more negative potentials, injection into the Co_xO_y CB occurs.

Publications funded by DE-FG03-02ER15753 since 2007:

- Shallcross, R. C.; D'Ambruoso, G. D.; Korth, B. D.; Hall, H. K., Jr.; Zheng, Z.; Pyun, J.; Armstrong, N. R. Poly(3,4-ethylenedioxythiophene) Semiconductor nanoparticle composite thin films tethered to indium tin oxide substrates via electropolymerization. *Journal of the American Chemical Society* 2007, 129, 11310-11311.
- 2. Shallcross, R. C.; D'Ambruoso, G. D.; Pyun, J.; Armstrong, N. R. Photoelectrochemical Processes in Polymer-Tethered CdSe Nanocrystals. *Journal of the American Chemical Society* **2010**, *132*, 2622-2632.
- 3. Shallcross, R. C.; Chawla, G. S.; Marikkar, F. S.; Tolbert, S.; Pyun, J.; Armstrong, N. R. Efficient CdSe Nanocrystal Diffraction Gratings Prepared by Microcontact Molding. *Acs Nano* **2009**, *3*, 3629-3637.
- Keng, P. Y.; Kim, B. Y.; Shim, I.-B.; Sahoo, R.; Veneman, P. E.; Armstrong, N. R.; Yoo, H.; Pemberton, J. E.; Bull, M. M.; Griebel, J. J.; Ratcliff, E. L.; Nebesny, K. G.; Pyun, J. Colloidal Polymerization of Polymer-Coated Ferromagnetic Nanoparticles into Cobalt Oxide Nanowires. Acs Nano 2009, 3, 3143-3157.

- Kim, B. Y.; Shim, I.-B.; Araci, Z. O.; Saavedra, S. S.; Monti, O. L. A.; Armstrong, N. R.; Sahoo, R.; Srivastava, D. N.; Pyun, J. Synthesis and Colloidal Polymerization of Ferromagnetic Au-Co Nanoparticles into Au-Co3O4 Nanowires. *Journal of the American Chemical Society* 2010, 132, 3234-3235.
- 6. Keng, P. Y.; Bull, M. M.; Shim, I.-B.; Nebesny, K. G.; Armstrong, N. R.; Sung, Y.; Char, K.; Pyun, J. Colloidal Polymerization of Polymer-Coated Ferromagnetic Cobalt Nanoparticles into Pt-Co(3)O(4) Nanowires. *Chemistry of Materials* **2011**, *23*, 1120-1129.
- 7. Kim, B. Y.; Shallcross, R. C.; Armstrong, N. R.; Kim, H. J.; Chung, W. J.; Sahoo, R.; Char, K.; Dirlam, P. T.; Costanzo, P. J.; Pyun, J.: Surface Intiated Atom Transfer Radical Polymerizations from Indium Tin Oxide Electrodes: Electrochemistry of Polymer Brushes. In *Progress in Controlled Radical Polymerization: Materials and Applications*; Matyjaszewski, K., Sumerlin, B. S., Tsarevsky, N. V., Eds.; ACS Symposium Series, 2012; Vol. 1101; pp 197-+.
- 8. Araci, Z. O.; Shallcross, C. R.; Armstrong, N. R.; Saavedra, S. S. Potential-Modulated Attenuated Total Reflectance Characterization of Charge Injection Processes in Monolayer-Tethered CdSe Nanocrystals. *Journal of Physical Chemistry Letters* **2010**, *1*, 1900-1905.
- Ehamparam, R.; Pavlopoulos, N. G.; Liao, M. W.; Hill, L. J.; Armstrong, N. R.; Pyun, J.; Saavedra, S. S. Band Edge Energetics of Heterostructured Nanorods: Photoemission Spectroscopy and Waveguide Spectroelectrochemistry of Au-Tipped CdSe Nanorod Monolayers. *Acs Nano* 2015, 9, 8786-8800.
- Wu, K.; Hill, L. J.; Chen, J.; McBride, J. R.; Pavlopolous, N. G.; Richey, N. E.; Pyun, J.; Lian, T. Universal Length Dependence of Rod-to-Seed Exciton Localization Efficiency in Type I and Quasi-Type II CdSe@CdS Nanorods. ACS Nano 2015, 9, 4591-4599.
- 11. Pavlopolous, N. G.; Dubose, J.; Lu, Y.; Huang, X.; Pinna, N.; Willinger, M.-G.; Lian, T.; Char, K.; Pyun, J. Type I vs Quasi-Type II Modulation in CdSe@CdS Tetrapods: Ramifications for Noble Metal Tipping. *ACS Nano* **2017**, *submitted*.
- 12. Hill, L. J.; Bull, M. M.; Sung, Y.; Simmonds, A. G.; Dirlam, P. T.; Richey, N. E.; DeRosa, S. E.; Shim, I.-B.; Guin, D.; Costanzo, P. J.; Pinna, N.; Willinger, M.-G.; Vogel, W.; Char, K.; Pyun, J. Directing the Deposition of Ferromagnetic Cobalt onto Pt-Tipped CdSe@CdS Nanorods: Synthetic and Mechanistic Insights. *Acs Nano* **2012**, *6*, 8632-8645.
- 13. Hill, L. J.; Pyun, J. Colloidal Polymers via Dipolar Assembly of Magnetic Nanoparticle Monomers. *Acs Applied Materials & Interfaces* **2014**, *6*, 6022-6032.
- 14. Hill, L. J.; Richey, N. E.; Sung, Y.-H.; Dirlam, P. T.; Lavoie-Higgins, E.; Shim, I.-B.; Pinna, N.; Willinger, M.-G.; Vogel, W.; Char, K.; Pyun, J. Colloidal Polymers via Dipolar Assembly of Heterostructured Co-tipped CdSe@CdS Nanorods. *ACS Nano* **2014**, *8*, 3272-3284.
- Hill, L. J.; Richey, N. E.; Sung, Y.-H.; Dirlam, P. T.; Lavoie-Higgins, E.; Shim, I.-B.; Pinna, N.;
 Willinger, M.-G.; Vogel, W.; Char, K.; Pyun, J. Synthesis and Dipolar Assembly of
 Heterostructured Cobalt Tipped CdSe@CdS Nanorods. Cryst. Eng. Comm. 2014, 16, 9461-9468.
- 16. Pavlopoulos, N. G.; Dubose, J. T.; Pinna, N.; Willinger, M. G.; Char, K.; Pyun, J. Synthesis and Assembly of Dipolar Heterostructured Tetrapods: Colloidal Polymers with "Giant tert-butyl" Groups. *Angewandte Chemie-International Edition* **2016**, *55*, 1787-1791.

17. Liao, M. W.; Pavlopoulos, N. G.; Hill, N. J.; Pyun, J.; Saavedra, S. S.; Armstrong, N. R. Band Edge Energies of Pt-Tipped CdSe@CdS Core@Shell Nanorods: New Approaches to Characterization of Complex Heterostructures with Photoemission Spectroscopies. *ACS Applied Materials and Interfaces* **2017**, *submitted*.